Weak localization in systems with chiral spin textures and skyrmion crystals

K. S. Denisov[1,2,*] and L. E. Golub[1]
[1]*Ioffe Institute, 194021 St. Petersburg, Russia*
[2]*School of Engineering Science, Lappeenranta-Lahti University of Technology, FI-53851 Lappeenranta, Finland*

(Received 11 March 2019; revised manuscript received 15 May 2019; published 19 July 2019)

A theory of interference-induced quantum corrections to conductivity is developed for two-dimensional systems with chiral spin textures including skyrmions. The effect of exchange interaction between electrons and spin textures on weak localization of electronic waves is studied. The spin dephasing rates are calculated as functions of the spin texture size. The anomalous magnetoresistance is shown to be governed by the size and magnetization spatial distribution of the spin textures. The effect of average magnetization-induced spin splitting on weak localization is analyzed. The sign-alternating weak-antilocalization magnetoresistance is demonstrated for skyrmion crystals. We argue that analysis of the low-field magnetoresistance might assist the experimental detection of chiral spin textures and, in particular, skyrmions.

DOI: 10.1103/PhysRevB.100.014424

I. INTRODUCTION

The past decade has featured an impressive rise in chiral magnetism. Various chiral spin textures, such as magnetic skyrmions [1–5] and antiskyrmions [6,7], skyrmion lattices [8,9], and merons and bimerons [10–12] are being extensively studied both experimentally and theoretically. The interest is especially sparked by the fact that the chiral nature of such textures opens up a novel area of physics with a number of intriguing phenomena, such as the topological Hall effect [13–17], its reciprocal analog—the skyrmion Hall effect [18,19], the anomalous Nernst effect [20], or nontrivial magnon-skyrmion interaction [21]. Moreover, it is believed that a chiral spin order would manifest itself in a whole variety of solid-state phenomena related to spin interactions.

The electric transport in media with spin skyrmions or other chiral spin textures is modified due to an exchange interaction between itinerant carriers and localized spins forming such textures. A carrier propagating in space and interacting with spin textures experiences rotations of its spin. For instance, when a texture size is comparable with the electron de Broglie wavelength, the interaction with textures results in spin-dependent electron scattering [22,23] leading to spin relaxation. In particular, the interference between single and double electron scattering events inside one chiral spin texture generates the transverse electron flux leading to the Hall response [13,22–24]. On the other hand, in systems with strong exchange interaction, such as skyrmion crystals, an electron spin is coaligned everywhere with local magnetization, which results in the formation of a purely geometrical effective magnetic field acting on its orbital motion and also leading to the Hall effect.

Spin-dependent phenomena are known to affect electron transport in metallic systems due to the weak localization effect (WL) [25,26]. Anomalous magnetoresistance in classically low magnetic fields is caused by magnetoinduced breaking of interference of electron waves passing scattering paths related by time inversion. The spin dependence of the scattering amplitude results in dramatic changes of the quantum conductivity correction up to the change of its sign, a phenomenon also known as weak antilocalization. The anomalous magnetoresistance is enhanced in systems with a not extremely large product $k_F\ell$, where k_F is the Fermi wave vector and ℓ is the mean free path. In systems with chiral spin textures, ℓ typically does not exceed tens of nanometers [27,28], which suggests the importance of the interference corrections.

In two-dimensional (2D) systems, the weak localization to antilocalization transitions are studied mainly in semiconductor heterostructures with spin-orbit splitting of the energy spectrum; for a review, see Ref. [29]. Investigations of the spin-flip scattering effect on WL are performed for structure-asymmetric *n*-type nonmagnetic and magnetic heterostructures [30–32] and for systems with spin-orbit scattering [33–37]. In this work, we demonstrate that the low-field magnetoresistance in systems with spin textures is featured by a specific behavior that cannot be attributed to either spin-orbit or magnetic-impurity scattering, thus its experimental observation would unambiguously indicate the presence of chiral spin order in a system.

In this paper, we theoretically investigate the WL effect in 2D systems with chiral spin textures. We start with a description of WL for the disordered array of spin textures, when each texture causes an additional carrier scattering; see the inset to Fig. 1. Then we investigate the case of a skyrmion crystal, assuming that skyrmions form a regular lattice. We demonstrate that the chiral spin pattern in real space affects the magnetoresistivity differently, depending upon its spatial size and the inner structure. Our results suggest that the presence of chiral spin textures can affect the low-field magnetoresistance.

*denisokonstantin@gmail.com

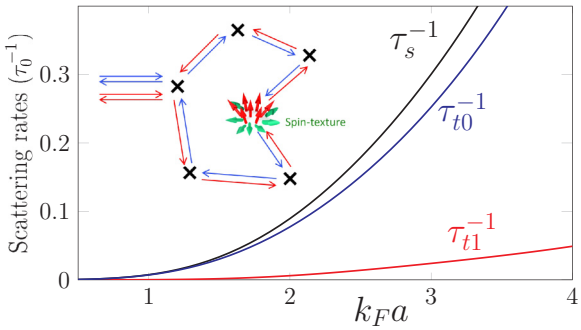

FIG. 1. The dependence of the scattering rates for singlet (τ_s^{-1}) and triplet ($\tau_{t0,t1}^{-1}$) channels on a spin texture radius for the spin spatial distribution Eq. (11) with $\alpha = \pi/2$. The inset shows two time-inverted electron trajectories with scattering by both impurities and a spin texture.

II. DISORDERED ARRAY OF CHIRAL SPIN TEXTURES

We consider a 2D layer containing randomly distributed chiral spin textures with the spin profile $\boldsymbol{S}(\boldsymbol{r})$ of the following shape:

$$\boldsymbol{S}(\boldsymbol{r}) = (\boldsymbol{S}_\parallel(r,\phi), S_z(r)), \quad S_x \pm iS_y = S_\parallel(r)e^{\pm i(\chi\phi+\gamma)}, \quad (1)$$

where $S_z, S_\parallel$ are the spin texture out-of-plane and in-plane components, respectively, and the characteristic radius of each textures is a. The textures are featured by the in-plane rotation of spin, and the parameters describing this rotation (χ and phase γ) are determined by a microscopic mechanism behind its formation [38]. For instance, when a chiral spin pattern appears due to a spin-orbit interaction, its rotation is given by $|\chi| = 1$ for linear and $|\chi| = 3$ for cubic in momentum spin-orbit splitting of a carrier spectrum [39].

We assume that the magnetization contains a homogeneous part $S_0\boldsymbol{e}_z$ normal to the 2D plane and the deviation of magnetization $\delta\boldsymbol{S}(\boldsymbol{r}) = \boldsymbol{S}(\boldsymbol{r}) - S_0\boldsymbol{e}_z$. The Hamiltonian of the electron exchange interaction with the spin texture is given by

$$\hat{\mathcal{H}} = -h_{\rm ex}S_0\hat{\sigma}_z - \sum_i h_{\rm ex}\hat{\boldsymbol{\sigma}}\cdot\delta\boldsymbol{S}(\boldsymbol{r}-\boldsymbol{R}_i), \quad (2)$$

where $h_{\rm ex}$ is the exchange interaction constant, $\hat{\boldsymbol{\sigma}}$ is the vector of Pauli matrices, and the sum runs over spin textures located in random points $\boldsymbol{R}_i$.

In our model, the 2D electron band structure consists of two parabolas shifted by $\Delta \equiv 2|h_{\rm ex}S_0|$, so the spin-up and spin-down electrons at the Fermi level have different Fermi wave vectors $k_{\rm F1,2} = \sqrt{2M(E_{\rm F} \pm \Delta/2)}/\hbar$, with $E_{\rm F}$ and M being the Fermi energy and electron effective mass, respectively. In what follows, we assume that the mean free path $\ell_{1,2}$ within each spin subband is determined by electron scattering by nonmagnetic impurities. There are two distinct regimes of weak localization depending on the relation between Δ and $\ell_{1,2}$. If the difference $|k_{\rm F1} - k_{\rm F2}|$ is much smaller than the inverse scattering lengths $1/\ell_{1,2}$, then the coherence between the spin-split subbands is important, and one can neglect the presence of spin splitting Δ. In the opposite case $|k_{\rm F1} - k_{\rm F2}| \gg \ell_{1,2}^{-1}$ the coherence is preserved only inside the subbands, and the spin-flip scattering acts as additional dephasing. In this paper, we consider both of these regimes.

A. Subband coherent WL

We start with the WL effect for the coherent subbands regime $|k_{\rm F1} - k_{\rm F2}| \ll \ell_{1,2}^{-1}$. The conductivity correction for 2D systems in a weak perpendicular magnetic field $\boldsymbol{B}$ is given by [26]

$$\Delta\sigma(B) = \frac{e^2}{2\pi h}\left[2f_2\left(\frac{B}{B_{t1}}\right) + f_2\left(\frac{B}{B_{t0}}\right) - f_2\left(\frac{B}{B_s}\right)\right], \quad (3)$$

where $f_2(x) = \psi(1/2 + 1/x) + \ln x$, with ψ being the digamma function. The characteristic magnetic fields for singlet (B_s) and triplet states with the angular momentum projection equal to 0 and 1 ($B_{t0,t1}$) are as follows:

$$B_i = B_\phi\left(1 + \frac{\tau_\phi}{\tau_i}\right), \qquad i = t1, t0, s, \quad (4)$$

where τ_ϕ is the dephasing time, and the characteristic magnetic field $B_\phi = \hbar\tau/(2|e|\ell^2\tau_\phi)$, where ℓ and τ are the mean free path and transport scattering time in the subbands. Additional dephasing described by the three times $\tau_{t1,t0,s}$ arises due to spin-dependent scattering by spin textures. Note that when there is no spin relaxation ($1/\tau_i = 0$), the correction to the conductivity coincides with a standard curve:

$$\Delta\sigma_0(B) = \frac{e^2}{\pi h}f_2(B/B_\phi). \quad (5)$$

The amplitude of electron elastic scattering in a system with the textures and ordinary impurities has the form

$$\hat{V}_{\boldsymbol{k}\boldsymbol{k}'} = V_0\hat{I}\sum_j e^{i\boldsymbol{q}\cdot\boldsymbol{\rho}_j} - h_{\rm ex}k_F^{-2}\hat{\boldsymbol{\sigma}}\cdot\boldsymbol{m}(\boldsymbol{q})\sum_i e^{i\boldsymbol{q}\cdot\boldsymbol{R}_i}, \quad (6)$$

where $\boldsymbol{q} = \boldsymbol{k} - \boldsymbol{k}'$, $\hat{I}$ is the 2×2 unit matrix, and V_0 is the amplitude of spin-independent scattering by impurities located in the points $\boldsymbol{\rho}_j$. The function $\boldsymbol{m}(\boldsymbol{q})$ is the Fourier transform of a spin texture $\delta\boldsymbol{S}(\boldsymbol{r})$:

$$m_x(\boldsymbol{q}) \pm im_y(\boldsymbol{q}) = -ie^{\mp i(\chi\varphi_q+\gamma)}m_\parallel(q),$$
$$m_{z,\parallel}(q) = 2\pi k_{\rm F}^2\int_0^\infty dr\, rJ_{0,\chi}(qr)\delta S_{z,\parallel}(r), \quad (7)$$

where J_l is the Bessel functions of the lth order.

The presence of in-plane components of a spin texture $m_{x,y}$ leads to a finite electron spin relaxation rate unless an electron spin becomes adiabatically coupled with a local magnetization, which occurs at $4h_{\rm ex}a/v_F\hbar \gg 1$. In the latter case, the spin-flip scattering is adiabatically suppressed, and the WL correction is described by the standard curve $\Delta\sigma_0(B)$, Eq. (5). In our model, by contrast, we treat the electron scattering by spin textures perturbatively, assuming $4h_{\rm ex}a/v_F\hbar \lesssim 1$. As a result, the spin-relaxation rate for the electron spin z-component is finite, which modifies the WL corrections.

The correlator of the spin-dependent scattering potential relevant for the WL problem has the form [26,31]

$$\left[n_i|V_0|^2 + \mathcal{N}\left(h_{\rm ex}k_F^{-2}\right)^2|\boldsymbol{m}(\boldsymbol{q})|^2\right]\hat{I} - \langle\hat{V}_{\boldsymbol{k}\boldsymbol{k}'}\otimes\hat{V}_{-\boldsymbol{k},-\boldsymbol{k}'}\rangle, \quad (8)$$

where angular brackets denote averaging over the impurity and texture positions, which are assumed to be not correlated; here n_i and $\mathcal{N}$ are the sheet densities of ordinary impurities and spin textures, respectively. We also assume that $\ell \gtrsim a$ not addressing the case of multiple scattering events inside one

spin texture, as the latter can restore the adiabatic regime and suppress a spin relaxation [40].

It follows from Eqs. (7) that m_z is invariant while $m_{x,y}$ change their signs under the operation $\boldsymbol{k}, \boldsymbol{k}' \to -\boldsymbol{k}, -\boldsymbol{k}'$. This differs the scattering by spin textures from both magnetic-impurity and spin-orbit scattering where $\hat{V}_{-\boldsymbol{k},-\boldsymbol{k}'} = \hat{V}_{\boldsymbol{k}\boldsymbol{k}'}$. Introducing the operator of unit angular momentum $\hat{\boldsymbol{J}}$, we obtain that the spin-dephasing rates are the eigenvalues of the following operator:

$$2\overline{\left(m_z^2 + m_\parallel^2\right)}\hat{I} - 2\overline{m_z^2}\hat{J}_z^2 - \overline{m_\parallel^2}\left(\hat{J}_x^2 + \hat{J}_y^2\right). \tag{9}$$

Here $m_{z,\parallel}$ depend on $q = 2k_\mathrm{F}\sin|(\varphi_{\boldsymbol{k}} - \varphi_{\boldsymbol{k}'})/2|$, and the lines mean averaging over both the initial and final angles $\varphi_{\boldsymbol{k}}$ and $\varphi_{\boldsymbol{k}'}$. We have taken into account that $m_{x,y}$ are pure imaginary and m_z is real, see Eqs. (7), and we use the following relations:

$$\overline{m_i m_j} = \overline{m_i^2}\delta_{ij}, \quad \overline{m_{x,y}^2} = -\overline{|m_{x,y}|^2} = -\tfrac{1}{2}\overline{m_\parallel^2}.$$

For the singlet ($\hat{J}_i = 0$) and triplet states, we obtain [41]

$$\frac{1}{\tau_{t0}} = \frac{2}{\tau_0}\overline{m_z^2}, \quad \frac{1}{\tau_{t1}} = \frac{1}{\tau_0}\overline{m_\parallel^2}, \quad \frac{1}{\tau_s} = \frac{1}{\tau_{t0}} + \frac{2}{\tau_{t1}}, \tag{10}$$

where we introduced the characteristic spin-flip rate $1/\tau_0 = 2\pi\mathcal{N}\nu h_{\mathrm{ex}}^2/(\hbar k_F^4)$ ($\nu = M/2\pi\hbar^2$ is the 2D density of states). We also assume that the transport scattering rate $\tau^{-1} = (2\pi/\hbar)n_i\nu|V_0|^2$ is determined by ordinary impurities. The dephasing times $\tau_{s,t0,t1}$ can be related with the single-particle spin relaxation times for spin orientation out of (τ_z) and in ($\tau_\parallel$) the 2D plane by $1/\tau_z = 2/\tau_{t1}$ and $1/\tau_\parallel = 1/\tau_{t0} + 1/\tau_{t1}$.

The obtained expressions demonstrate that, since $1/\tau_s > 1/\tau_{t0,t1}$, the singlet contribution [last term in Eq. (3)] is smaller than that from the triplet channel. Therefore, the sign of the magnetoconductivity correction is positive at any size of a spin texture, $\Delta\sigma(B) > 0$. However, the form of the magnetoresistance curves strongly depends both on the texture size and the Fermi energy, revealing a number of distinct features induced by the chiral character of spin arrangement [42].

We proceed by considering the shape of $\Delta\sigma(B)$ curves for different chiral spin textures $\boldsymbol{S}(\boldsymbol{r})$. Let us mention that for a spin texture with $S_\parallel = 0$ (a magnetic impurity with spin directed perpendicular to the 2D plane) we have $1/\tau_{t1} = 0$ and $\tau_s = \tau_{t0}$, the relaxation of the z spin component is absent, and the WL correction is given by $\Delta\sigma_0(B)$; see Eq. (5). To analyze the effect of the chiral spin texture in-plane spin rotation on $\Delta\sigma(B)$ curves, we provide the numerical calculations for the following texture shape:

$$\begin{pmatrix}\delta S_z(r)\\ \delta S_\parallel(r)\end{pmatrix} = (1-x)^2\Theta(1-x)\begin{pmatrix}\cos\alpha x\\ \sin\alpha x\end{pmatrix}, \tag{11}$$

where $x = r/a$, with a being the texture radius, α controls the in-plane spin inclination, and Θ is the Heaviside function (we assume that $\delta S_{z,\parallel} = 0$ outside a texture core). The texture shape Eq. (11) is convenient for quantifying the considered phenomenon allowing us to demonstrate the effect of the texture magnetization inclination on WL. In Fig. 1 we plot the dependence of $\tau_{s,t0,t1}^{-1}$ on $k_F a$ for $\delta S_{z,\parallel}$ profiles [Eq. (11)] at $\alpha = \pi/2$. The increase of a texture radius leads to a more efficient spin-flip scattering and larger τ_{t1}^{-1} rate. When all three times $\tau_{s,t0,t1}$ become different, the magnetoconductivity correction changes strongly.

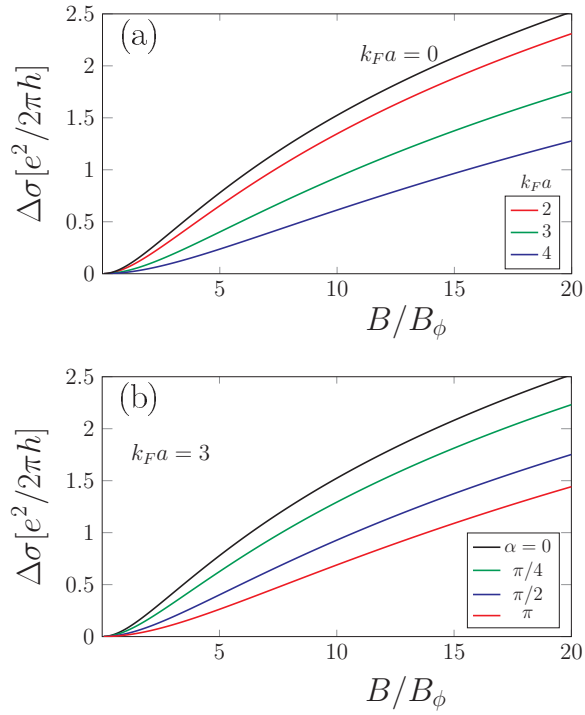

FIG. 2. The magnetic field dependence of the weak-localization conductivity correction at $\tau_\phi/\tau_0 = 30$ for (a) a different spin texture radius $k_F a$ (at $\alpha = \pi/2$) and (b) a different spin inclination angle α (at $k_F a = 3$).

Figure 2(a) demonstrates $\Delta\sigma(B)$ for a different texture radius, suggesting that an increase of the texture size suppresses effectively the conductivity correction. The inner structure of a spin texture also affects the magnetoresistance. The larger the spin inclination angle is, and correspondingly the more intense the spin-flip scattering rates are, the more pronounced is the suppression of $\Delta\sigma(B)$. In Fig. 2(b) we plot $\Delta\sigma(B)$ for four different spin configurations described by $\alpha = 0$, $\pi/4$, $\pi/2$, and π. This plot demonstrates the suppression of $\Delta\sigma(B)$ as the spin texture is tilted into the plane.

B. Subband incoherent WL

Now we consider the case of large spin splitting assuming that $|k_{\mathrm{F}1} - k_{\mathrm{F}2}| \gg \ell_{1,2}^{-1}$. We characterize the spin-flip scattering by the scattering time τ_{12}, which is equal for scattering processes $1 \to 2$ and $2 \to 1$. The spin-flip scattering rate by a skyrmion coincides with the spin relaxation time of the triplet state with projection 1: $\tau_{12} = \tau_{t1}$; see Eq. (10). In contrast to the coherent subband regime considered previously, for $|k_{\mathrm{F}1} - k_{\mathrm{F}2}| \gg \ell_{1,2}^{-1}$ the spin texture in-plane components affect WL only by means of intersubband scattering processes τ_{12}, i.e., without phase factor couplings. Nevertheless, the change of skyrmion parameters affecting τ_{12} can still lead to a change of the magnetoresistivity curves.

Generally, the dephasing times $\tau_{\phi 1}, \tau_{\phi 2}$ and the elastic scattering times in the subbands $\tau_{1,2}$ are different due to their dependence on the Fermi wave vectors. However, for the parabolic subbands the density of states at the Fermi level does not depend on spin index, thus we have $\tau_1 = \tau_2 = \tau$. On the

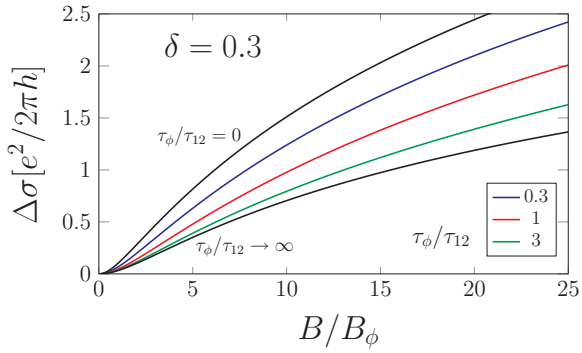

FIG. 3. The magnetic-field dependence of the conductivity correction for different spin-flip rates $1/\tau_{12}$. The 2D electron spin polarization $\delta = 0.3$.

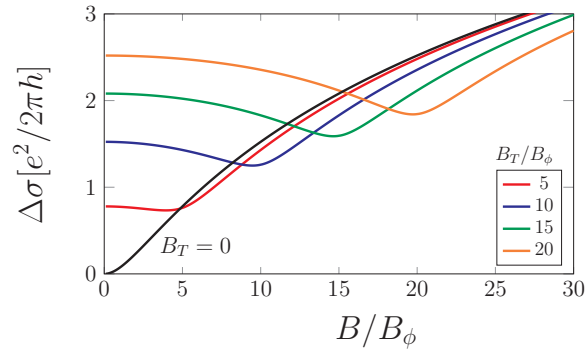

FIG. 4. The dependence of $\Delta\sigma(B)$ for skyrmion crystals with different values of the topological magnetic field B_T.

contrary, in each 2D subband the dephasing time is linear in the electron density. Therefore, we have $\tau_{\phi 1}, \tau_{\phi 2} = \tau_\phi(1 \pm \delta)$, where τ_ϕ is an average dephasing time, and $\delta = \Delta/2E_F$ is the 2D electron gas spin polarization.

As a result, we deal with the two-subband system with intersubband scattering. The weak-localization conductivity correction for this case is given by [34,35,43]

$$\Delta\sigma(B) = \frac{e^2}{2\pi h}\left[f_2\left(\frac{B}{B_+}\right) + f_2\left(\frac{B}{B_-}\right)\right],$$
$$B_\pm = \frac{B_\phi}{1-\delta^2}\left[\frac{\tau_\phi}{\tau_{12}} + p + 1 \pm \sqrt{\left(\frac{\tau_\phi}{\tau_{12}} + p\right)^2 + 2p}\right], \tag{12}$$

where $p = 2\delta^2/(1-\delta^2)$, and $B_\phi = \hbar/(2|e|v_F^2\tau\tau_\phi)$ is determined by the average dephasing time τ_ϕ and Fermi velocity $v_F = \sqrt{2E_F/M}$.

In Fig. 3 we demonstrate the evolution of the $\Delta\sigma(B)$ curves driven by the increase of τ_ϕ/τ_{12} for $\delta = 0.3$. If the intersubband scattering is slow in comparison with the dephasing rates in the subbands ($\tau_{12} \gg \tau_\phi$), then we obtain that spin subbands contribute independently with $B_\pm = B_\phi/(1 \mp \delta)^2$ corresponding to the second and first subbands, respectively. It is the 2D electron spin polarization δ that makes $B_\pm$ different in this case. Increasing the skyrmion size, we reduce the intersubband scattering time τ_{12}, thus approaching the opposite limit of fast spin-flips $\tau_{12} \ll \tau_\phi$ when we have two distinct characteristic fields given by an average dephasing rate and spin-flip rates, respectively: $B_- = B_\phi/(1-\delta^2)$ and $B_+ = (2\tau_\phi/\tau_{12})B_- \gg B_-$. As a result, the conductivity correction $\Delta\sigma$ is almost twice as small as that in the absence of spin-flip scattering. This is clearly seen from a comparison of the curves in Fig. 3 corresponding to $\tau_\phi/\tau_{12} = 0$ and to $\tau_\phi/\tau_{12} \to \infty$.

III. SKYRMION CRYSTALS

We proceed by considering an important case when skyrmions are spatially arranged in a regular lattice. In contrast to the above-considered diluted arrays of spin textures, the skyrmion crystal is characterized by a higher density of magnetic vortices so that $\mathcal{N}a^2 \lesssim 1$. We assume the adiabatic electron interaction with skyrmions, i.e., that an electron spin state is coaligned everywhere with a local magnetization and the skyrmions do not lead to the spin-flip scattering ($\tau_{12} = \infty$). This assumption is typical when considering the electron transport in real skyrmion crystals [9,44,45]. The chiral spatial structure of the magnetization manifests itself as a gauge contribution [15] to the operator of momentum: $\boldsymbol{p} \to \boldsymbol{p} \mp (e/c)\boldsymbol{A}(\boldsymbol{r})$, where the sign corresponds to two electron spin subbands, and $\boldsymbol{A}(\boldsymbol{r})$ is determined by a particular spin profile. The vector potential $\boldsymbol{A}(\boldsymbol{r})$ leads to the "topological" magnetic field acting on electron orbital motion. Its averaged component perpendicular to the 2D plane is given by

$$B_T = \frac{\phi_0}{4\pi}\langle \boldsymbol{S}\cdot[\partial_x\boldsymbol{S}\times\partial_y\boldsymbol{S}]\rangle \equiv Q\frac{\phi_0}{\mathcal{A}}, \tag{13}$$

where $\phi_0 = hc/|e|$ is a magnetic flux quantum, Q is an integer number, and $\mathcal{A}$ is an area of the crystal unit cell. Let us note that the sign of the emerging magnetic field $\pm B_T$ is opposite for two electron subbands, which modifies the anomalous magnetoresistance in a nontrivial way.

It is worth noting that the assumption of spin adiabaticity ($\tau_{12} = \infty$) is typical for a strong exchange interaction when the condition $|k_{F1} - k_{F2}| \gg \ell_{1,2}^{-1}$ is additionally fulfilled. As a result, the electrons from different subbands contribute to the conductivity independently, with the corresponding total magnetic field being a superposition of the external field B and the topological one B_T:

$$\Delta\sigma(B) = \frac{e^2}{2\pi h}\left[f_2\left(\frac{B+B_T}{B_\phi}\right) + f_2\left(\frac{B-B_T}{B_\phi}\right)\right]. \tag{14}$$

Here we assume equal dephasing times in the spin subbands, and that $\ell \gtrsim 2a$, so each electron indeed experiences an average magnetic field.

Figure 4 shows the dependence of $\Delta\sigma(B)$ on the external magnetic field B for a different ratio B_T/B_ϕ. This dependence is hallmarked by the emergence of a noticeable dip starting from $B_T/B_\phi \approx 4$. The position of this minimum is unambiguously associated with the magnitude of the topological field B_T.

IV. DISCUSSION AND SUMMARY

The considered theory of WL corrections in a dilute array of chiral spin textures is valid when $\ell \gtrsim a$. With a typical

mean free path limited by tens of nanometers, we conclude that the described features of WL are important for systems with compact spin textures and, in particular, skyrmions. For instance, this is the case of nanoscale skyrmions observed in atomically thin magnetic layers, such as PdFe/Ir(111) [1]. Another example is diluted magnetic semiconductors (DMS) with the size of spin textures being of the order of the impurity Bohr radius [39]. It is also worth estimating the spin-flip times given by Eq. (10) and comparing them with the dephasing time τ_ϕ for those systems. For DMS, the subband-coherent regime is typically realized. Taking $h_{\rm ex} = 2$ meV, the electron sheet density $N_{2D} = k_F^2/(2\pi) = 4 \times 10^{12}$ cm^{-2}, the spin texture density $\mathcal{N} = 10^{12}$ cm^{-2}, and $M = 0.1m_0$, we obtain the characteristic spin-flip time $\tau_0 \approx 0.5$ ns. For the dephasing time $\tau_\phi = 10$ ns and the texture radius $a = 5$ nm we get $\tau_\phi/\tau_0 \approx 20$ and $k_F a \approx 2.5$, which suggests the importance of WL corrections. Other relevant systems are atomically thin ferromagnetic films, featured by a large exchange splitting of electron spin subbands. Taking $h_{\rm ex} = 0.5$ eV, $N_{2D} = 10^{14}$ cm^{-2}, and the transport scattering time $\tau = 1$ ps, we get for the ratio $h_{\rm ex}\tau/\hbar \approx 10^3$, which suggests that the WL corrections are described by the theory of the subband-incoherent regime Eq. (12). For $\mathcal{N} = 10^{10}$ cm^{-2} and $M = 0.6m_0$ we get the spin-flip time $\tau_0 \approx 0.1$ ns, and for $\tau_\phi = 1$ ns and $a = 2$ nm we obtain $\tau_\phi/\tau_0 \approx 10$ and $k_F a \approx 4$. Therefore, according to Eq. (12), the WL correction is expected to be twice as small as the standard result Eq. (5).

Let us estimate the effective topological field for skyrmion crystals. Taking $a = 20$ nm, we get $B_T \approx 3$ T, which is one to two orders of magnitude larger than typical values of B_ϕ. As a result, a very narrow dip is expected in the $\Delta\sigma(B)$ dependence (Fig. 4). We note that the other transport phenomenon takes place in skyrmion crystals, namely the topological Hall effect. Therefore, we argue that when the topological Hall effect is experimentally observed, the longitudinal conductivity would also experience a modification due to WL according to Eq. (14).

In summary, we developed the WL theory for 2D electron systems with chiral spin textures. We demonstrated that, in disordered arrays of spin textures, the WL is featured by a specific behavior that cannot be attributed to any other mechanism. For skyrmion crystals, the sign-alternating magnetoresistance is predicted.

ACKNOWLEDGMENTS

The financial support of the Russian Science Foundation (Project No. 17-12-01265) and the Foundation for Advancement of Theoretical Physics and Mathematics ("BASIS") is acknowledged.

[1] R. Wiesendanger, Nanoscale magnetic skyrmions in metallic films and multilayers: A new twist for spintronics, Nat. Rev. Mater. **1**, 16044 (2016).

[2] A. Fert, N. Reyren, and V. Cros, Magnetic skyrmions: Advances in physics and potential applications, Nat. Rev. Mater. **2**, 17031 (2017).

[3] A. Soumyanarayanan, M. Raju, A. L. G. Oyarce, A. K. C. Tan, M.-Y. Im, A. P. Petrović, P. Ho, K. H. Khoo, M. Tran, C. K. Gan *et al.*, Tunable room-temperature magnetic skyrmions in Ir/Fe/Co/Pt multilayers, Nat. Mater. **16**, 898 (2017).

[4] S. D. Pollard, J. A. Garlow, J. Yu, Z. Wang, Y. Zhu, and H. Yang, Observation of stable Néel skyrmions in cobalt/palladium multilayers with lorentz transmission electron microscopy, Nat. Commun. **8**, 14761 (2017).

[5] T. Lin, H. Liu, S. Poellath, Y. Zhang, B. Ji, N. Lei, J. J. Yun, L. Xi, D. Z. Yang, T. Xing, Z. L. Wang, L. Sun, Y. Z. Wu, L. F. Yin, W. B. Wang, J. Shen, J. Zweck, C. H. Back, Y. G. Zhang, and W. S. Zhao, Observation of room-temperature magnetic skyrmions in Pt/Co/W structures with a large spin-orbit coupling, Phys. Rev. B **98**, 174425 (2018).

[6] A. K. Nayak, V. Kumar, T. Ma, P. Werner, E. Pippel, R. Sahoo, F. Damay, U. K. Rößler, C. Felser, and S. S. P. Parkin, Magnetic antiskyrmions above room temperature in tetragonal heusler materials, Nature (London) **548**, 561 (2017).

[7] M. Hoffmann, B. Zimmermann, G. P. Müller, D. Schürhoff, N. S. Kiselev, C. Melcher, and S. Blügel, Antiskyrmions stabilized at interfaces by anisotropic Dzyaloshinskii-Moriya interactions, Nat. Commun. **8**, 308 (2017).

[8] S. Mühlbauer, B. Binz, F Jonietz, C. Pfleiderer, A. Rosch, A. Neubauer, R. Georgii, and P. Böni, Skyrmion lattice in a chiral magnet, Science **323**, 915 (2009).

[9] C. S. Spencer, J. Gayles, N. A. Porter, S. Sugimoto, Z. Aslam, C. J. Kinane, T. R. Charlton, F. Freimuth, S. Chadov, S. Langridge, J. Sinova, C. Felser, S. Blügel, Y. Mokrousov, and C. H. Marrows, Helical magnetic structure and the anomalous and topological Hall effects in epitaxial B20 $Fe_{1-y}Co_yGe$ films, Phys. Rev. B **97**, 214406 (2018).

[10] X. Z. Yu, W. Koshibae, Y. Tokunaga, K. Shibata, Y. Taguchi, N. Nagaosa, and Y. Tokura, Transformation between meron and skyrmion topological spin textures in a chiral magnet, Nature (London) **564**, 95 (2018).

[11] B. Göbel, A. Mook, J. Henk, I. Mertig, and O. A. Tretiakov, Magnetic bimerons as skyrmion analogues in in-plane magnets, Phys. Rev. B **99**, 060407(R) (2019).

[12] Y. A. Kharkov, O. P. Sushkov, and M. Mostovoy, Bound States of Skyrmions and Merons Near the Lifshitz Point, Phys. Rev. Lett. **119**, 207201 (2017).

[13] G. Tatara and H. Kawamura, Chirality driven anomalous Hall effect in weak coupling regime, J. Phys. Soc. Jpn. **71**, 2613 (2002).

[14] T. Taniguchi, K. Yamanaka, H. Sumioka, T. Yamazaki, Y. Tabata, and S. Kawarazaki, Direct Observation of Chiral Susceptibility in the Canonical Spin Glass AuFe, Phys. Rev. Lett. **93**, 246605 (2004).

[15] P. Bruno, V. K. Dugaev, and M. Taillefumier, Topological Hall Effect and Berry Phase in Magnetic Nanostructures, Phys. Rev. Lett. **93**, 096806 (2004).

[16] M. Raju, A. Yagil, A. Soumyanarayanan, A. K. C. Tan, A. Almoalem, O. M. Auslaender, and C. Panagopoulos, Evolution of chiral magnetic textures and their topological Hall signature in Ir/Fe/Co/Pt multilayer films, Nat. Commun. **10**, 696 (2019).

[17] K. S. Denisov, I. V. Rozhansky, N. S. Averkiev, and E. Lähderanta, General theory of the topological Hall effect in

systems with chiral spin textures, Phys. Rev. B **98**, 195439 (2018).

[18] K. Everschor-Sitte and M. Sitte, Real-space Berry phases: Skyrmion soccer, J. Appl. Phys. **115**, 172602 (2014).

[19] W. Jiang, X. Zhang, G. Yu, W. Zhang, X. Wang, M. B. Jungfleisch, J. E. Pearson, X. Cheng, O. Heinonen, K. L. Wang *et al.*, Direct observation of the skyrmion Hall effect, Nat. Phys. **13**, 162 (2017).

[20] X. Li, L. Xu, L. Ding, J. Wang, M. Shen, X. Lu, Z. Zhu, and K. Behnia, Anomalous Nernst and Righi-Leduc Effects in Mn_3Sn: Berry Curvature and Entropy Flow, Phys. Rev. Lett. **119**, 056601 (2017).

[21] S.-Z. Lin, C. D. Batista, C. Reichhardt, and A. Saxena, Ac Current Generation in Chiral Magnetic Insulators and Skyrmion Motion Induced by the Spin Seebeck Effect, Phys. Rev. Lett. **112**, 187203 (2014).

[22] K. S. Denisov, I. V. Rozhansky, N. S. Averkiev, and E. Lähderanta, Electron Scattering on a Magnetic Skyrmion in the Nonadiabatic Approximation, Phys. Rev. Lett. **117**, 027202 (2016).

[23] H. Ishizuka and N. Nagaosa, Spin chirality induced skew scattering and anomalous Hall effect in chiral magnets, Sci. Adv. **4**, eaap9962 (2018).

[24] K. Nakazawa and H. Kohno, Weak coupling theory of topological Hall effect, Phys. Rev. B **99**, 174425 (2019).

[25] J. Rammer, *Quantum Transport Theory* (Westview, Boulder, CO, 2004).

[26] S. Hikami, A. I. Larkin, and Y. Nagaoka, Spin-orbit interaction and magnetoresistance in the two dimensional random system, Prog. Theor. Phys. **63**, 707 (1980).

[27] J. Zang, M. Mostovoy, J. H. Han, and N. Nagaosa, Dynamics of Skyrmion Crystals in Metallic Thin Films, Phys. Rev. Lett. **107**, 136804 (2011).

[28] R. G. Elías, N. Vidal-Silva, and A. Manchon, Steady motion of skyrmions and domains walls under diffusive spin torques, Phys. Rev. B **95**, 104406 (2017).

[29] M. M. Glazov and L. E. Golub, Spin-orbit interaction and weak localization in heterostructures, Semicond. Sci. Technol. **24**, 064007 (2009).

[30] K. S. Romanov and N. S. Averkiev, Anomalous magnetoresistance of two-dimensional systems in the presence of spin-orbit scattering, J. Exp. Theor. Phys. **101**, 699 (2005).

[31] F. V. Porubaev and L. E. Golub, Weak localization in low-symmetry quantum wells, Phys. Rev. B **90**, 085314 (2014).

[32] I. Garate, J. Sinova, T. Jungwirth, and A. H. MacDonald, Theory of weak localization in ferromagnetic (Ga,Mn)As, Phys. Rev. B **79**, 155207 (2009).

[33] N. S. Averkiev, V. A. Berezovets, G. E. Pikus, N. I. Sablina, and I. I. Farbshtein, Quantum corrections to 2D hole conductivity in a quantum well on Te $(10\bar{1}0)$, Phys. Solid State **40**, 1409 (1998).

[34] N. S. Averkiev, L. E. Golub, and G. E. Pikus, Anomalous magnetoresistance in p-type quantum wells, Solid State Commun. **107**, 757 (1998).

[35] N. S. Averkiev, L. E. Golub, and G. E. Pikus, Weak localization in p-type quantum wells, Semiconductors **32**, 1087 (1998).

[36] W.-Yu. Shan, H.-Z. Lu, and S.-Q. Shen, Spin-orbit scattering in quantum diffusion of massive Dirac fermions, Phys. Rev. B **86**, 125303 (2012).

[37] F. V. Porubaev and L. E. Golub, Weak localization of holes in high-mobility heterostructures, Phys. Rev. B **87**, 045306 (2013).

[38] N. Nagaosa and Y. Tokura, Topological properties and dynamics of magnetic skyrmions, Nat. Nanotechnology **8**, 899 (2013).

[39] K. S. Denisov and N. S. Averkiev, Hall effect driven by noncollinear magnetic polarons in diluted magnetic semiconductors, Appl. Phys. Lett. **112**, 162409 (2018).

[40] K. Nakazawa, M. Bibes, and H. Kohno, Topological Hall effect from strong to weak coupling, J. Phys. Soc. Jpn. **87**, 033705 (2018).

[41] The spin dephasing rates $1/\tau_{t0,t1}$ in the triplet channel are calculated by diagonalization of the 3-rank matrix (9). Using the relation $\hat{J}_x^2 + \hat{J}_y^2 = 2\hat{I} - \hat{J}_z^2$ valid for the triplet states we get the operator Eq. (9) in the following form: $2\overline{m_z^2}\hat{I} + (\overline{m_\parallel^2} - 2\overline{m_z^2})\hat{J}_z^2$. This yields Eq. (10).

[42] For systems with randomly oriented magnetic impurities, all three times are determined by one spin-flip scattering parameter $\overline{m_z^2} = \overline{m_{x,y}^2}$. By contrast, in the studied systems with spin textures, the dephasing rates are different and even can differ by an order of magnitude.

[43] N. S. Averkiev, L. E. Golub, S. A. Tarasenko, and M. Willander, Effect of intersubband scattering on weak localization in two-dimensional systems, Phys. Rev. B **64**, 045405 (2001).

[44] A. Neubauer, C. Pfleiderer, B. Binz, A. Rosch, R. Ritz, P. G. Niklowitz, and P. Böni, Topological Hall Effect in the *a* Phase of MnSi, Phys. Rev. Lett. **102**, 186602 (2009).

[45] Y. Li, N. Kanazawa, X. Z. Yu, A. Tsukazaki, M. Kawasaki, M. Ichikawa, X. F. Jin, F. Kagawa, and Y. Tokura, Robust Formation of Skyrmions and Topological Hall Effect Anomaly in Epitaxial Thin Films of MnSi, Phys. Rev. Lett. **110**, 117202 (2013).